

## Article

# Effect of Cr and Al on Elastic Constants of FeCrAl Alloys Investigated by Molecular Dynamics Method

Hui Dai <sup>1</sup>, Miaosen Yu <sup>1</sup>, Yibin Dong <sup>1</sup>, Wahyu Setyawan <sup>2</sup>, Ning Gao <sup>1,3,\*</sup> and Xuelin Wang <sup>1</sup>

<sup>1</sup> Institute of Frontier and Interdisciplinary Science and Key Laboratory of Particle Physics and Particle Irradiation (MOE), Shandong University, Qingdao 266237, China; huidai@mail.sdu.edu.cn (H.D.); 202120966@mail.sdu.edu.cn (M.Y.); ybdong@mail.sdu.edu.cn (Y.D.); xuelinwang@sdu.edu.cn (X.W.)

<sup>2</sup> Pacific Northwest National Laboratory, Richland, WA 99352, USA; wahyu.setyawan@pnnl.gov

<sup>3</sup> Institute of Modern Physics, Chinese Academy of Sciences, Lanzhou 730000, China

\* Correspondence: ning.gao@sdu.edu.cn

**Abstract:** The FeCrAl alloy system is recognized as one of the candidate materials for accident-tolerant fuel (ATF) cladding in the nuclear power industry due to its high oxidation resistance under irradiation and high-temperature environments. The concentrations of Cr and Al have a significant effect on elastic properties of the FeCrAl alloy. In this work, elastic constants  $C_{11}$ ,  $C_{12}$ ,  $C_{44}$ , bulk modulus and shear modulus of FeCrAl alloy were calculated with molecular dynamics methods. We explored compositions with 1–15 wt.% Cr and 1–5 wt.% Al at temperatures from 0 K to 750 K. The results show that the concentrations of Al and Cr have different effects on the elastic constants. When the concentration of Al was fixed, a decrease in bulk modulus and shear modulus with increasing Cr content was observed, consistent with previous experimental results. The dependence of elastic constants on temperature was also the same as in the experiments. Investigations into elastic properties of defect-containing alloys have shown that vacancies, voids, interstitials and Cr-rich precipitations have different effects on elastic properties of FeCrAl alloys. Investigations of elastic properties of defect-containing alloys have shown that vacancies, void, interstitials and Cr-rich precipitations have different effects on elastic properties of FeCrAl alloys. Therefore, the present results indicate that both the Cr and Al concentrations and radiation defects should be considered to develop and apply the FeCrAl alloy in ATF design.

**Keywords:** FeCrAl; elastic properties; temperature effect; molecular dynamics



**Citation:** Dai, H.; Yu, M.; Dong, Y.; Setyawan, W.; Gao, N.; Wang, X. Effect of Cr and Al on Elastic Constants of FeCrAl Alloys Investigated by Molecular Dynamics Method. *Metals* **2022**, *12*, 558. <https://doi.org/10.3390/met12040558>

Academic Editor: Angelo Fernando Padilha

Received: 18 January 2022

Accepted: 22 March 2022

Published: 25 March 2022

**Publisher's Note:** MDPI stays neutral with regard to jurisdictional claims in published maps and institutional affiliations.



**Copyright:** © 2022 by the authors. Licensee MDPI, Basel, Switzerland. This article is an open access article distributed under the terms and conditions of the Creative Commons Attribution (CC BY) license (<https://creativecommons.org/licenses/by/4.0/>).

## 1. Introduction

After the Fukushima Daiichi nuclear power disaster in 2011, development of accident-tolerant fuels (ATF) has been in great demand to enhance the safety of nuclear power plants, especially under accident conditions [1]. In addition to coated claddings, FeCrAl cladding is one of the possible technologies for use in ATF. In the past few years, based on this concept, FeCrAl alloys have been extensively studied and the advantages have been recognized, including improved high-temperature steam oxidation resistance [2], resistance to radiation damages [3], strength under both normal conditions and high-temperature accident conditions [4], and enhanced corrosion performance under normal conditions [5].

The roles of Cr and Al elements have been explored to understand the above properties. For example, Cr is added to improve the water corrosion resistance of these alloys at normal operating temperatures, and Al is added to improve the high-temperature oxidation resistance of the alloy through the formation of protective  $\alpha$ -Al<sub>2</sub>O<sub>3</sub> [6,7]. However, it should also be noted that various properties of FeCrAl alloys are strongly affected by the addition and concentrations of Cr and Al, including the mechanical properties. For example, the  $\alpha'$  phase in FeCrAl alloy will nucleate and grow at temperatures around 475 °C with a concentration of Cr,  $C_{Cr}$ , around 10~18 at.%, which leads to embrittlement of the alloy under normal conditions [8,9]. Meanwhile, under irradiation, the  $\alpha'$  phase could

form even at 320 °C, with  $C_{Cr}$  around 10~18 at.% [10]. Hence, it is necessary to decrease the concentration of Cr to reduce the  $\alpha'$  phase formation and related embrittlement of the alloy under irradiation at medium temperatures [11]. For this purpose, Oak Ridge National Laboratory (ORNL) has prepared a variety of FeCrAl-Y alloys with different Cr concentrations to develop new low-Cr, high-strength FeCrAl-Y alloys [11]. They found that a FeCrAl alloy with  $C_{Cr}$  less than 13 wt.% can effectively avoid the formation of a brittle phase at 475 °C. Gussev et al. found that adding Al to the alloy can improve the oxidation resistance, but the higher Al concentration,  $C_{Al}$ , increases, the greater the difficulty of welding and manufacturing the FeCrAl alloys [8,12].

In addition, previous studies have also reported that the concentration of Cr and Al could significantly affect the mechanical properties of FeCrAl alloys [12]. The elastic properties have been investigated for evaluating the survivability of cladding materials under energetic neutron irradiation [13]. In fact, mechanical properties, including the elastic modulus, yield stress, ultimate tensile stress, and so on, have been generally measured and estimated for selection of structural materials used in reactors before neutron irradiation experiments [14,15]. For example, before irradiation, it was reported by Liu et al. that the increase in Cr concentration will enhance the bulk modulus of the alloy. However, when the concentration of Al increases from 4.5 wt.% to 6 wt.%, the bulk modulus could also slightly decrease [14]. From experimental viewpoints, Speich et al. measured the shear modulus  $G$ , the ratio of the bulk modulus to the shear modulus  $K/G$ , and the Poisson's ratio  $\nu$  [16] using an ultrasonic pulse echo repeat method [17] at 298 K, indicating that the shear modulus and Poisson's ratio of the Fe-rich region of the Fe-Cr alloy showed a linear dependence with the increase of Cr concentration. Harmouche et al. prepared FeAl-B2 phase samples with Fe atomic fractions from 50.87% to 60.2%, and by measuring its Young's modulus at room temperature, the authors found that the dependence of Young's modulus on the concentration of Fe shows a quadratic relationship [18]. The dependence of elastic modulus, Poisson's ratio, and shear modulus on temperature has also been explored for FeCrAl alloy and almost no variation has been observed as a function of major alloy elements [12]. Based on the above literature review, it is clear that although there are many studies on the mechanical properties of binary alloys, research on the elastic properties of ternary alloys needs to be enriched, especially on the mutual effect of Cr and Al on the elastic constants of a ternary FeCrAl alloy. From the viewpoint of fundamental research, it would be necessary to investigate the Cr and Al concentration effect from the lower to higher values in order to present the possible dependence of elastic properties on these alloy elements.

Different from the effect of Cr and Al on mechanical properties before the irradiation, the effect of radiation-induced defects on the mechanical properties of FeCrAl alloy is another key factor in evaluating the performance of the selected material. From previous studies, it is well known that the elastic modulus is one of important parameters to be dynamically measured in order to estimate the state of structure materials during the performance of nuclear reactors [13]. Thus, understanding the elastic constant and modulus before and after the irradiation is important for the development and further optimization of FeCrAl alloys used in ATF design. Under irradiation, the super-saturated interstitials, vacancies, voids, and precipitates are generally observed, which are expected to affect the mechanical properties of FeCrAl alloys. For example, the formation of Cr-rich  $\alpha'$  phases in irradiated FeCrAl alloys has been investigated by small-angle neutron scattering (SANS) [19,20], atom probe tomography (APT) [21,22], high-efficiency STEM-EDS (energy-dispersive spectroscopy) [21] and a series of technical studies. Unfortunately, although the irradiation hardening and embrittlement of FeCrAl after irradiation have been investigated, the detailed dependence of elastic constants or modulus on irradiation defects in FeCrAl alloys is not well understood, so research comparing this to the dynamically measured elastic modulus of materials to increase the safe operation of nuclear reactors would be valuable.

Therefore, in order to shed light on above questions, in this work, molecular dynamics (MD) simulations have been performed to calculate the elastic constants of FeCrAl alloy with 1~15 wt.% Cr and 1~5 wt.% Al at different temperatures (0 K, 300 K, 450 K, 600 K and 750 K) to understand the concentration effect of alloy elements on elastic properties of FeCrAl alloy. The effects of radiation defects, including vacancies, interstitials and Cr precipitates on the elastic properties, are also simulated. Through these calculations, the elastic properties of FeCrAl alloy before and after the irradiation can be understood from an atomic scale. In the rest of this paper, the method of calculations is introduced in Section 2, results and discussion are provided in Section 3, and conclusion is given in the last section.

## 2. Methods

In this work, molecular dynamics (MD) simulations have been performed with LAMMPS software to calculate the elastic constants at different temperatures. The computational box was built with three directions along [100], [010] and [001]. There are 10 unit cells along each direction, thus, 2000 atoms in the matrix box. The interactions between atoms in FeCrAl are described by the F-S potential developed by Liao et al., which has been shown to be accurate to describe the characteristics of the elements in FeCrAl alloys [22]. The time step is 1 femtosecond (fs), and the total simulation time is up to 10 ps for each simulation.

The elastic tensor can be written as a  $6 \times 6$  matrix using the Voigt concept, that is,  $C_{ij}$  instead of  $C_{ijkl}$ . According to this definition, during calculations, the elastic constants can be calculated by applying elementary deformations in the six distinct strain components and measuring the changes in the six stress components accordingly. In this work, the strain to induce the deformation of the simulation box was set as  $10^{-6}$ . Thus, according to the dependence of stress on strain, the elastic constants can be calculated. For temperatures higher than 0 K, thermal motion is included in the calculation of the stress. For the cubic lattice simulated in this work, the elastic tensor has three independent elastic constants, namely  $C_{11}$ ,  $C_{12}$  and  $C_{44}$ . With the above method, these elastic constants can be calculated with or without temperature effect. In fact, this method has been applied by different groups to investigate the elastic properties of materials. For example, Miller et al. studied the elastic constants of PbTe, SnTe and  $\text{Ge}_{0.08}\text{Sn}_{0.92}\text{Te}$  with this method [23]. In order to understand the influence of solute atoms on the elastic constants of FeCrAl alloys, 1~15 wt.% Cr and 1~5 wt.% Al atoms were introduced as substitutional solutes to form a solid solution, since FeCrAl alloys generally form a solid solution, as observed in previous experiments [10,24]. For convenience, the atomic concentration, at.%, is usually applied for atomic simulations. The conversion between wt.% and at.% can be obtained by including the atomic mass for Fe, Cr and Al. Examples of this unit conversion are listed in Table 1. It should also be noted that both Cr and Al atoms were introduced into the computational box in a randomly substitutional way by keeping the distance between each pair of substitutional atoms at least one lattice constant. As stated above, simulations at different temperatures (0 K, 300 K, 450 K, 600 K, 750 K) were performed to explore the effect of temperature on the elastic constants of the alloy. Furthermore, at each temperature, 50 simulations were performed to get reliable statistics and to estimate uncertainties in the results.

**Table 1.** Examples of conversion from wt.% to at.% for several FeCrAl alloys.

Solute Element	Fe1Cr1Al			Fe2Cr5Al			Fe5Cr3Al			Fe8Cr5Al			Fe13Cr5Al		
	Fe	Cr	Al	Fe	Cr	Al									
wt.%	98	1	1	93	2	5	92	5	3	87	8	5	82	13	5
at.%	97	1	2	88	2	10	89	5	6	82	8	10	77	13	10

In addition, in order to consider the effect of vacancies, interstitials and Cr precipitates on elastic constants, a big simulation model with 36,000 atoms was built with three directions in the same orientation as before. The radiation-induced vacancies (and voids) are included in the computational box by changing,  $n$ , the number of vacancies in each vacancy

cluster or void and,  $m$ , the number of vacancy clusters or voids. For convenience, in this work, the total number of vacancies in the box was kept as 320, and thus  $nm = 320$ . The value of  $m$  is defined as 1, 2, 4, 5, 10, 20, 40, 80, 160 and 320, thus  $n$  is calculated accordingly. To investigate the effect of interstitials, different numbers of separated interstitials were in the computational box. For a single interstitial, the  $\langle 110 \rangle$  Fe-Fe or Fe-Cr dumbbell was built after the construction of FeCrAl alloy since the substitutional Al has lower formation energy, and thus, only the Fe-Fe and Fe-Cr dumbbells were built in the present work. As to the effect of Cr-rich  $\alpha'$  on elastic properties, similar to the model of vacancy clusters, the precipitates containing different numbers of Cr atoms were considered. The number of precipitates was 1 to 7 and two cases with a total number Cr atoms in the box up to 4300 ( $C_{Cr} \sim 11\%$ ) and 4850 ( $C_{Cr} \sim 13\%$ ), respectively, were considered. Following above method, simulations at 0 K were performed to explore the effects of vacancies, interstitials and Cr precipitates on the elastic constants of the alloys. In each case, 50 simulations were also performed to obtain reliable statistics and estimate the uncertainty in the results.

### 3. Results and Discussion

#### 3.1. Dependence of Elastic Constants on Concentration of Cr and Al

The calculated elastic constants,  $C_{11}$ ,  $C_{12}$ ,  $C_{44}$  and related bulk modulus and shear modulus, of FeCrAl alloy as a function of concentration of Cr and Al at 0 K are shown in Figure 1. The statistical uncertainties of these elastic constants and modulus were also calculated, which showed a similar dependence on concentration of Cr and Al, and thus just one example is presented in Figure 1f. Each panel in Figure 1 has five curves, corresponding to the five different concentrations of Al from 1 wt.% to 5 wt.%. For each curve, the data are plotted as a function Cr concentration from 1 wt.% to 15 wt.%. Some curves show an increasing trend, while others exhibit an opposite trend, indicating different dependencies of elastic constants on the concentrations of Al and Cr.

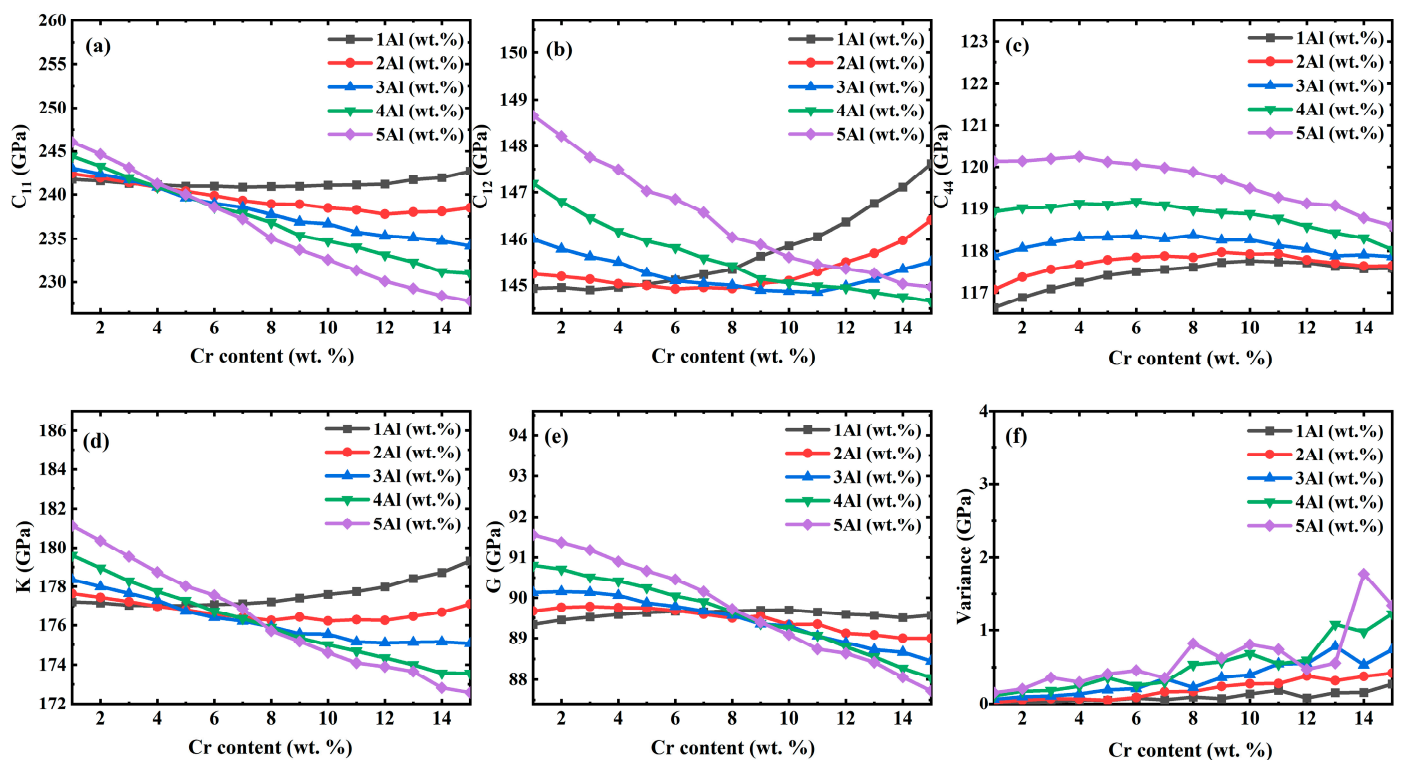


**Figure 1.** (a–e) Dependence of elastic constants,  $C_{11}$ ,  $C_{12}$ ,  $C_{44}$ , bulk modulus and shear modulus on Cr and Al concentrations at 0 K. (f) Example of statistical uncertainties for these elastic constants based on 50 simulations.

As shown in Figure 1a, for the lowest concentration of Al at 1 wt.%,  $C_{11}$  increases slightly with Cr concentration up to 15 wt.%. While for 2 to 5 wt.% Al,  $C_{11}$  decreases accordingly. Furthermore, from Figure 1a, when  $C_{Cr}$  is in the range of 1–3 wt.%,  $C_{11}$  increases with the increase of  $C_{Al}$ , while the opposite is true for  $C_{Cr}$  in the range of 5–15 wt.%. Interestingly, all curves intersect at a common point at 4 wt.% Cr, indicating that at this Cr concentration,  $C_{11}$  does not depend on  $C_{Al}$ .

For  $C_{12}$ , as shown in Figure 1b, when  $C_{Al}$  is 1 wt.% or 2 wt.%,  $C_{12}$  increases with  $C_{Cr}$  from 1 to 15 wt.%. When  $C_{Al}$  is 3 wt.%,  $C_{12}$  decreases firstly and then increases with  $C_{Cr}$ . When  $C_{Al}$  is 4 wt.% or 5 wt.%,  $C_{12}$  decreases with  $C_{Cr}$ . Furthermore, when  $C_{Cr}$  is fixed and  $C_{Cr}$  is lower than 5 wt.%,  $C_{12}$  increases with the increase of  $C_{Al}$ . When  $C_{Cr}$  is in the range of 5–13 wt.%, there is no clear dependence on  $C_{Al}$  with a fixed  $C_{Cr}$ . For  $C_{44}$ , as shown in Figure 1c, when  $C_{Al}$  is fixed from 1 to 5 wt.%,  $C_{44}$  increases firstly to a peak value and then decreases with the increase of  $C_{Cr}$ . It should also be noted that the peak is a function of  $C_{Al}$ , that is, the higher  $C_{Al}$  the higher the peak, and that the peak occurs at a smaller  $C_{Cr}$ . When  $C_{Cr}$  is fixed,  $C_{44}$  increases with the increase of  $C_{Al}$ .

In addition, the bulk modulus ( $K$ ) and the shear modulus ( $G$ ) have also been calculated according to the relationship between the elastic constants and  $K$  and  $G$ , derived by Voigt [25], as shown in Figure 1d,e. It is clear that when  $C_{Al}$  is 1 wt.%, the bulk modulus increases with  $C_{Cr}$ , which is consistent with the results of previous studies [26], that is, the bulk modulus of the alloy increases with the increase of Cr content. When  $C_{Al}$  is 2 wt.%, the bulk modulus decreases firstly and then increases with  $C_{Cr}$ . When  $C_{Al}$  is higher than 2 wt.%, the bulk modulus decreases with the increase of  $C_{Cr}$ . When the concentration of Cr is fixed, the bulk modulus increases with the increase of  $C_{Al}$  for  $C_{Cr} < 4$  wt.%. For  $C_{Cr}$  in the range of 4–8 wt.%, the dependence of the bulk modulus on  $C_{Al}$  is not linear. For  $C_{Cr} > 8$  wt.%, the bulk modulus decreases with the increase of  $C_{Al}$ . Regarding the shear modulus  $G$ , at 1 wt.% Al, the shear modulus is almost a constant with  $C_{Cr}$ . When the concentration of Al is higher than 1 wt.%, the shear modulus decreases with the increase of  $C_{Cr}$ . From this figure, there is also a common intersection of the shear modulus curves at a critical Cr concentration (8 wt.%), similar to the case of  $C_{11}$  (at 4 wt.%). Thus, for  $C_{Cr} < 8$  wt.%, the shear modulus increases with Al content, while the opposite is true for  $C_{Cr} > 8$  wt.%.

### 3.2. Dependence of Elastic Constants on Temperature

The elastic constants and modulus calculated at 300 K are shown in Figure 2. As shown in Figure 2a, the dependence of  $C_{11}$  on  $C_{Cr}$  and  $C_{Al}$  is similar to the results obtained at 0 K, as shown in Figure 1a. For  $C_{12}$ , comparing to the results shown in Figure 1b, for  $C_{Al} < 4$  wt.%, a similar dependence of  $C_{12}$  on  $C_{Cr}$  can be observed, that is,  $C_{12}$  increases with  $C_{Cr}$ . However, for  $C_{Al}$  equal to 4 wt.% and 5 wt.%, different trends were obtained.  $C_{12}$  is almost a constant as a function of  $C_{Cr}$  for  $C_{Al} = 4$  wt.%. While for  $C_{Al} = 5$  wt.%,  $C_{12}$  decreases firstly with  $C_{Cr}$  up to around 7 wt.% and then remains almost constant, as shown in the Figure 2 b. Furthermore, for a fixed  $C_{Cr}$ ,  $C_{12}$  always increases with the increase of  $C_{Al}$ . For  $C_{44}$ ,  $C_{44}$  increases with the increase of both  $C_{Cr}$  and  $C_{Al}$ , a behavior that is different from the  $C_{44}$  at 0 K, as previously shown in Figure 1c. Compared to the results at 0 K, the bulk modulus shows a similar dependence on the concentration of Cr and Al, as shown in Figures 1d and 2d. The shear modulus also shows a similar trend, but the critical  $C_{Cr}$  concentration for  $G$  (the intersection point) has changed from ~8 to ~15 wt.%. From these results, especially from the bulk modulus and shear modulus, it can be estimated that from the mutual effects of Cr and Al concentration on elastic properties, the concentration of Al should be not higher than 3% and the related Cr concentration should be higher than 10% in the bulk FeCrAl alloys. However, it should also be noted that the above results were obtained only according to the effect of concentration of Cr and Al on elastic properties but without considering the other defects and related defect interactions. Furthermore, since the formation of  $Al_2O_3$  on the material surface is the main reason to increase the high-temperature oxidation resistance of FeCrAl alloy and addition of Cr is necessary to increase the corrosion resistance, the Cr and Al concentrations are expected to be higher

to satisfy this requirement. In fact, many researchers have suggested to add the other elements to increase the performance of FeCrAl alloy. Therefore, the optimization of Cr and Al concentration needs to consider various conditions, which is beyond the topic of the present paper. The optimization of FeCrAl alloy can be found elsewhere [26,27].

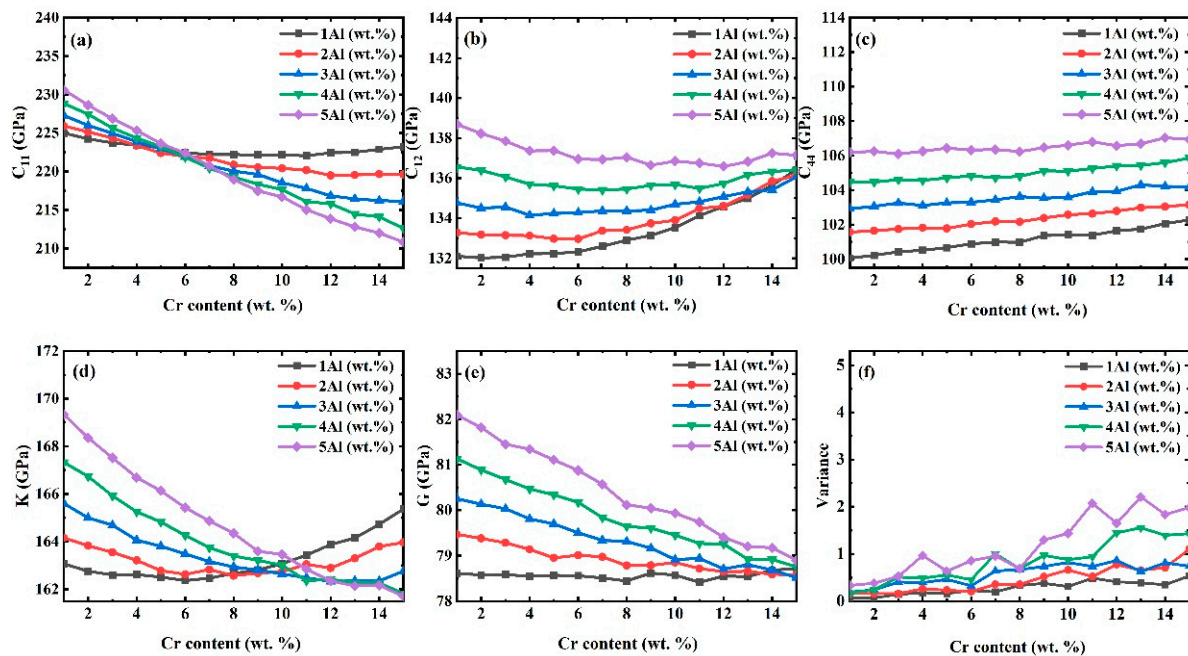


**Figure 2.** (a–e) Dependence of elastic constants,  $C_{11}$ ,  $C_{12}$ ,  $C_{44}$ , bulk modulus and shear modulus on Cr and Al concentration at 300 K. (f) Example of statistical uncertainty for these elastic constants based on 50 simulations.

In this work, as stated in the Methods section, the elastic constants and modulus at 450 K, 600 K and 750 K were also calculated. Detailed analysis indicates that the results obtained at different temperatures, including 0 K, 300 K, 450 K, 600 K and 750 K, show a similar dependence on the concentration of Cr and Al. One example for  $C_{Al} = 1$  wt.% is shown in Figure 3, which clearly indicates the same dependence of elastic constants on Cr and Al concentration at different temperatures. Therefore, based on these results, the dependence of elastic constants and modulus on temperature can be explored.

The dependence of elastic properties on temperature is shown in Figure 4. The results for alloys with 1 wt.% Al and 4 wt.%, 8 wt.% and 14 wt.% Cr, are shown to illustrate the temperature effect. From this figure, it is evident that all elastic constants investigated in this work,  $C_{11}$ ,  $C_{12}$ ,  $C_{44}$ , bulk modulus and shear modulus of these three alloys, decrease with increasing temperature from 300 K to 750 K, which is also consistent with the results of a previous study [27]. It is worth noting that in a previous experiment [28], the decrease of elastic constants with the increase of temperature has also been observed, in which the bulk modulus decreased from about 200 GPa at 300 K to about 150 GPa at 750 K, and the shear modulus decreased from about 77 GPa at 300 K to about 65 GPa at 750 K, both of which decreased by about 15% [28]. In the present work, the bulk and shear moduli decrease by about 6% and 9%, respectively, less than in the experiment. The main reason is that in the experiment, the sample was polycrystalline, while a single crystal is employed in our calculations. In a polycrystalline material, the effect of grain boundaries could contribute to the decrease of the elastic properties.

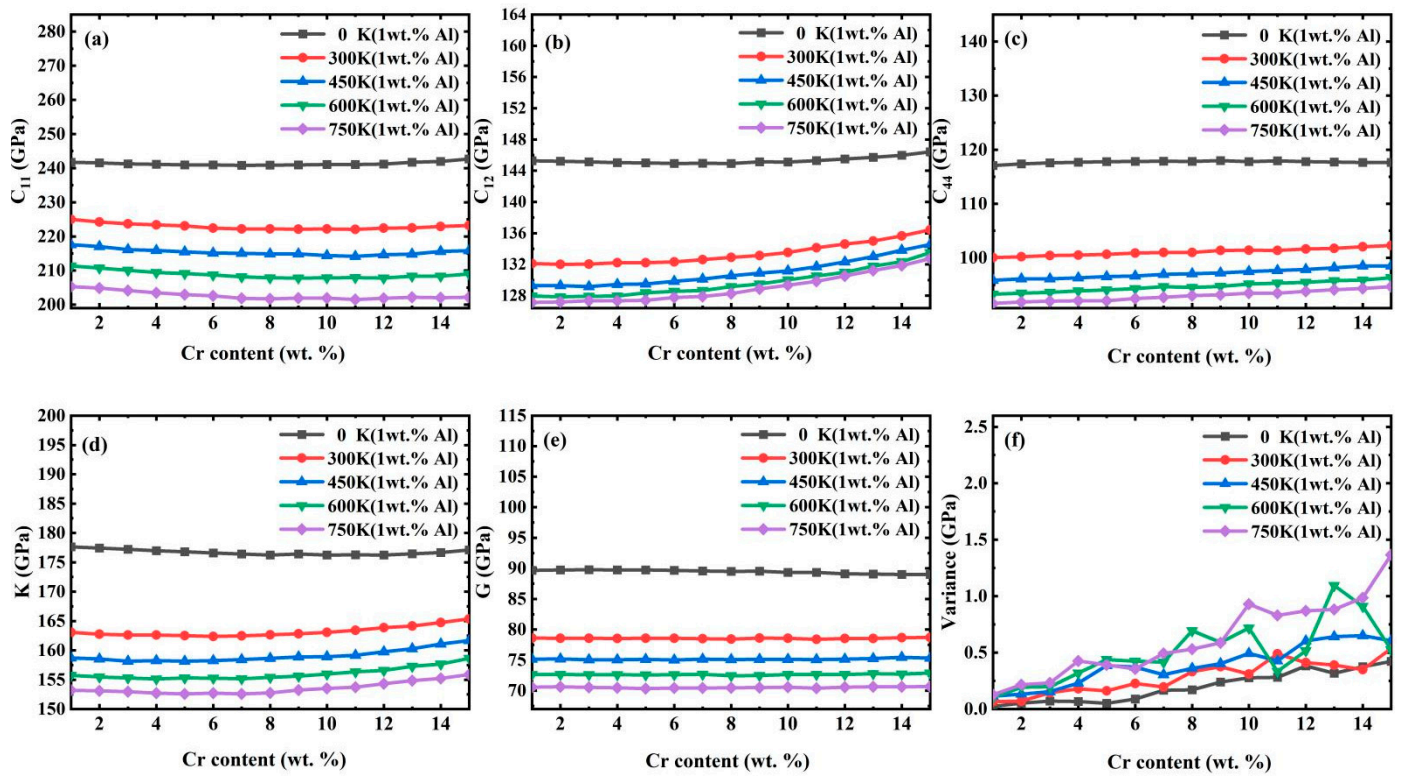


Figure 3. (a–e) Dependence of elastic constants,  $C_{11}$ ,  $C_{12}$ ,  $C_{44}$ , bulk modulus and shear modulus on the concentration of Cr in an FeCrAl alloy with 1 wt.% Al at temperatures 0~750 k, (f) example of statistical uncertainty for these elastic constants based on 50 simulations.

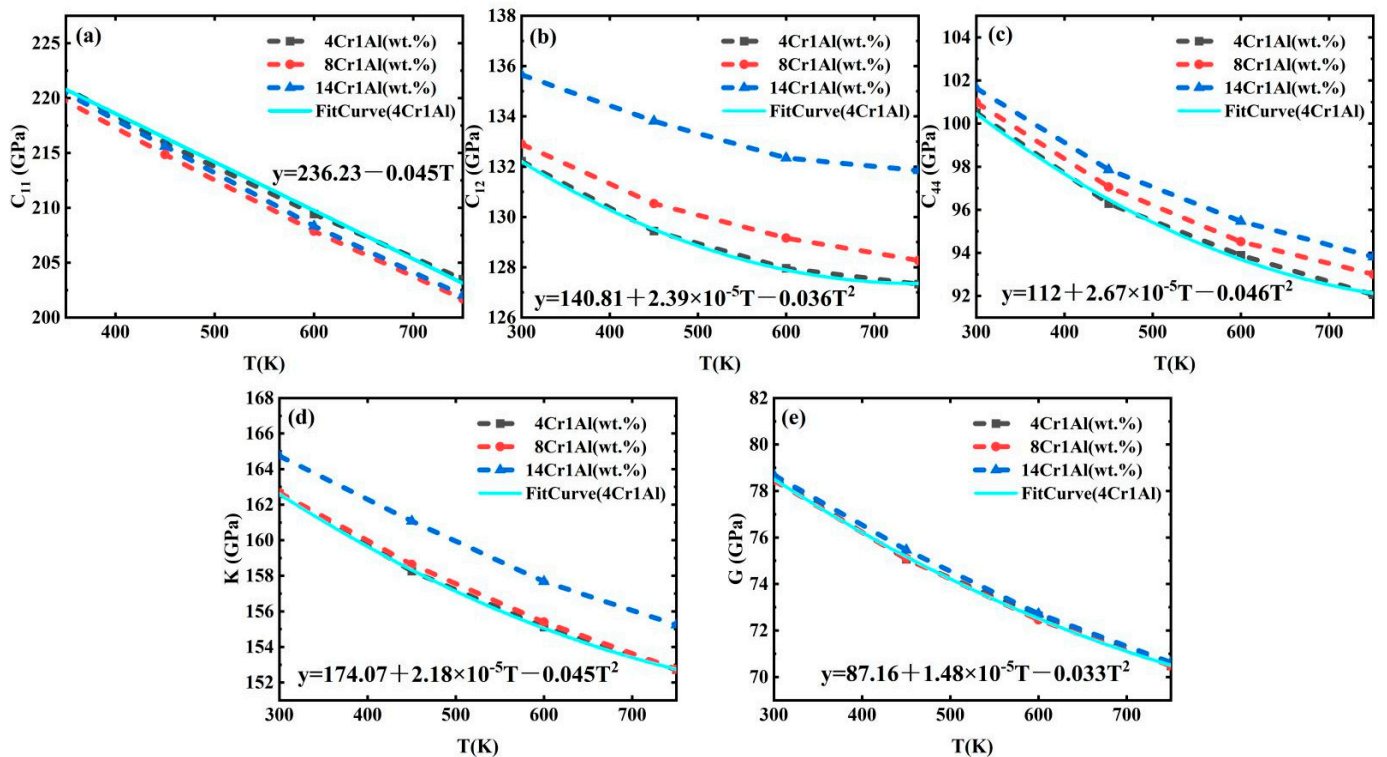


Figure 4. (a–e) Dependence of elastic constants,  $C_{11}$ ,  $C_{12}$ ,  $C_{44}$ , bulk modulus and shear modulus on temperature for 4Cr1Al (wt.%), 8Cr1Al (wt.%) and 14Cr1Al (wt.%) compositions at 300–750 K.

As shown in Figure 4, the dependence of each elastic constant on temperature follows the same trend for different concentration of Cr and Al, which, thus, can be described by the same equation but with different parameter values. For  $C_{11}$ , this dependence can be described as:

$$C_{11}(T) = A - BT \quad (1)$$

where  $A$  and  $B$  are parameters that depend on the concentration Cr and Al. For example, for 4Cr1Al (wt.%), 8Cr1Al (wt.%) and 14Cr1Al (wt.%),  $A$  is 236.23, 235.63 and 236.65 GPa, respectively, and  $B$  is 0.045, 0.045 and 0.047 GPa/K, respectively. The dependence of the other elastic constants,  $C_{12}$ ,  $C_{44}$ ,  $K$  and  $G$ , on temperature can be described by the following equation:

$$C(T) = A + BT - CT^2 \quad (2)$$

The fitted values for  $A$ ,  $B$  and  $C$  for different concentrations of Cr and Al are listed in Table 2. In Figure 4, the fitted equations for FeCrAl alloy with  $C_{Cr} \sim 4\%$ (wt.%) and  $C_{Al} \sim 1\%$ (wt.%) are also included.

**Table 2.** Fitted parameter values in the models of elastic constants and modulus as a function of temperature for Fe4Cr1Al (wt.%), Fe8Cr1Al (wt.%) and Fe14Cr1Al (wt.%). The models are given in Equations (1) and (2).

Solute	Fe4Cr1Al(wt.%)			Fe8Cr1Al(wt.%)			Fe14Cr1Al(wt.%)		
	A(GPa)	B(GPa/K)	C(GPa/K <sup>2</sup> )	A(GPa)	B(GPa/K)	C(GPa/K <sup>2</sup> )	A(GPa)	B(GPa/K)	C(GPa/K <sup>2</sup> )
$C_{11}$	236.23	0.045	/	235.63	0.045	/	236.65	0.047	/
$C_{12}$	140.81	$2.39 \times 10^{-5}$	0.036	139.61	$1.64 \times 10^{-5}$	0.027	141.60	$1.49 \times 10^{-5}$	0.024
$C_{44}$	112	$2.67 \times 10^{-5}$	0.047	112.25	$2.67 \times 10^{-5}$	0.046	112.11	$2.37 \times 10^{-5}$	0.042
$K$	174.07	$2.18 \times 10^{-5}$	0.045	172.68	$1.52 \times 10^{-5}$	0.038	174.18	$1.35 \times 10^{-5}$	0.035
$G$	87.16	$1.48 \times 10^{-5}$	0.033	87.20	$1.54 \times 10^{-5}$	0.034	86.90	$1.26 \times 10^{-5}$	0.031

The nature of the decrease in the elastic constant after the temperature rises is due to the change in the lattice constant caused by thermal expansion [13]. This phenomenon can also be understood from the elastic constant temperature dependence formula derived by Leibfried and Ludwig in 1961 [29].

### 3.3. Influence of Radiation Defects on Elastic Properties

The effects of different vacancy types on elastic properties are shown in Figure 5. According to experimental results, the concentrations of Cr and Al in FeCrAl are generally from 12 wt.% and 5% respectively. In this work, the Fe8Cr5Al and Fe13Cr5Al alloys were selected as examples to show the effects of radiation defects on elastic constants. From these figures, it is clear that after the formation of radiation-induced vacancies, the  $C_{11}$ ,  $C_{12}$ ,  $C_{44}$ , bulk modulus and shear modulus of these two alloys decrease in comparison to the perfect state. It should also be noted that when the vacancy clusters are formed, these elastic constants decrease slightly or are kept constants and then increase with an increase of vacancy cluster size but decrease of the number of vacancy clusters. The  $K/G$  value remains around 2.30, larger than 1.75, which is still a ductility alloy according to Pugh's rule [30].

The dependence of elastic properties on different numbers of dumbbell interstitials are shown in Figure 6 for Fe8Cr5Al and Fe13Cr5Al alloys. It is also clear that  $C_{11}$ ,  $C_{44}$  and shear modulus decrease when the interstitials are formed in these two alloys. However,  $C_{12}$  and bulk modulus increase when the number of interstitials increases, different from the results of  $C_{11}$ ,  $C_{44}$  and shear modulus. Therefore, according to the definitions of bulk and shear modulus, it can be understood from the present results that the formation of interstitials could increase the ability of the alloys to resist the volume change under the effect of pressure but decrease the ability to resist the torsion applied on alloys. When

the materials are applied in a nuclear reactor, the interaction between dislocations and these interstitials could further affect the mechanical properties. Thus, the present results indicate that the formation of an interstitial should be included, even if these interstitials are distributed separately and before their interaction with dislocations.

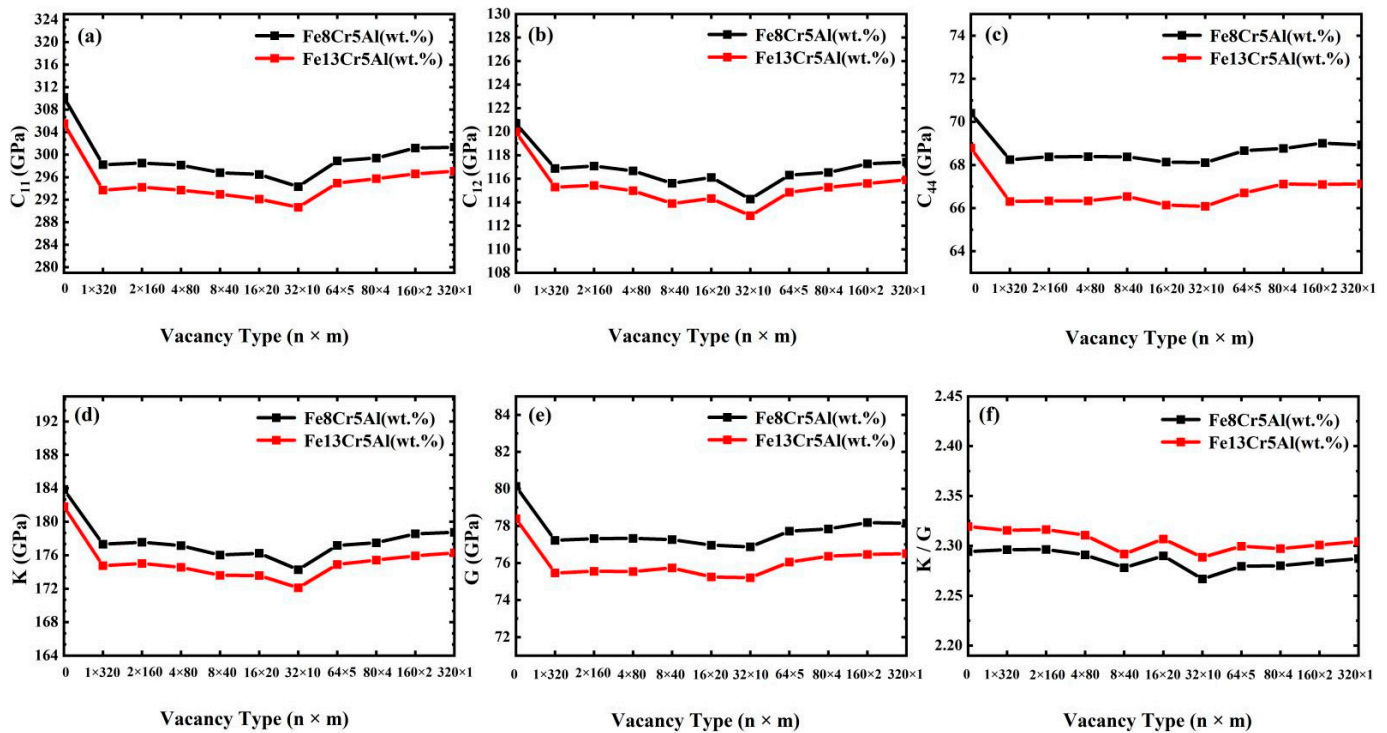


**Figure 5.** (a–e) The effects of vacancy and void on  $C_{11}$ ,  $C_{12}$ ,  $C_{44}$ , bulk modulus and shear modulus, (f) shows the value of  $K/G$  as a function of vacancy type. In these figures,  $n$  is the number of vacancies in each vacancy cluster or void and  $m$  is the number of vacancy clusters or voids.

When the Cr-rich precipitates are formed, the dependence of elastic properties on numbers of Cr precipitates are shown in Figure 7 for Fe8Cr5Al and Fe13Cr5Al alloys. From these results, it can be seen that after the Cr-rich precipitates are formed, these elastic properties of alloys increase but are kept as almost a constant, thus they are independent of the number and volume of precipitates. From previous studies, it is known that the precipitates would affect the mechanical properties. According to the present results, it can be understood that the effect of  $\alpha'$  precipitates on the mechanical properties of FeCrAl should be mainly due to their interaction with dislocations, different from the effects of vacancies, voids and interstitials, as shown in Figures 5 and 6. All results shown in Figures 5 and 6 indicate that an increase of Cr concentration would result in the decrease of elastic properties under the irradiation environment. Thus, the concentration of Cr in alloys should also be limited as indicated experimentally [3,9]. These results also indicate the radiation defects could result in larger decreases or increases of elastic properties than the Cr and Al concentrations. Furthermore, comparing the effects from vacancies, voids, interstitials and Cr-rich precipitates, it is clear that the interstitials have stronger effects on bulk and shear modulus than vacancies, voids and Cr-rich precipitates. It should also be noted the present results only consider the effects from radiation defects. The effect from the interaction between dislocations and radiation defects on mechanical properties should be investigated in future work.

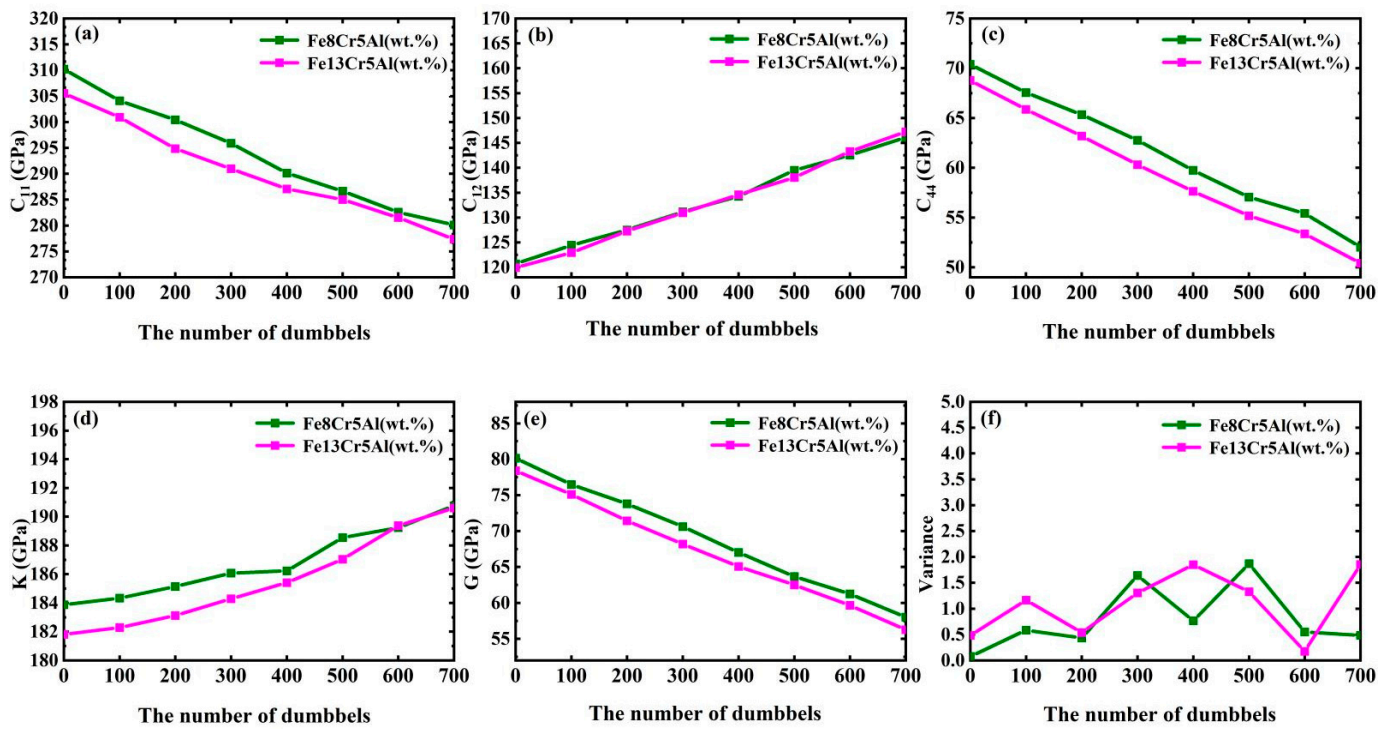


Figure 6. (a–e) The dependence of  $C_{11}$ ,  $C_{12}$ ,  $C_{44}$ , bulk modulus and shear modulus on number of dumbbell interstitials, (f) shows one example of statistical uncertainty for these elastic constants based on 50 simulations at 0 K.

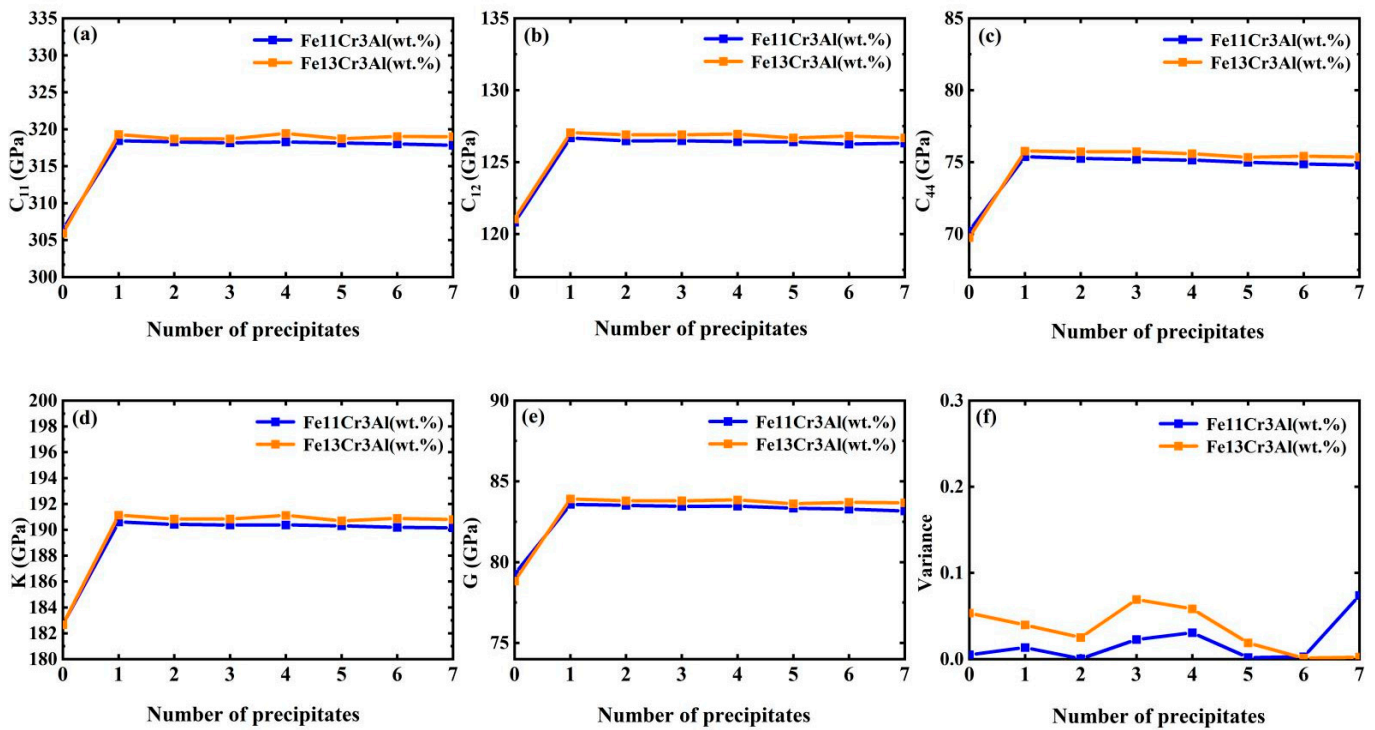


Figure 7. (a–e) The dependence of  $C_{11}$ ,  $C_{12}$ ,  $C_{44}$ , bulk modulus and shear modulus on number of Cr precipitates. (f) Example of statistical uncertainty for these elastic constants based on 50 simulations at 0 K.

#### 4. Conclusions

In this work, the elastic constants,  $C_{11}$ ,  $C_{12}$ ,  $C_{44}$ , bulk modulus and shear modulus of FeCrAl alloys were calculated with molecular dynamics methods for compositions with 1~15 wt.% Cr and 1~5 wt.% Al at temperatures from 0 K to 750 K. The effects of Cr and Al concentrations and temperature on elastic constants have been explored. The results indicate that  $C_{11}$ ,  $C_{12}$ ,  $C_{44}$ , bulk modulus and shear modulus show different dependencies on the concentrations of Cr and Al. In particular, for alloys with Al concentration >3 wt.%, the bulk modulus decreases with the increase of Cr concentration. However, for Al concentration of 1–5 wt.%, the shear modulus decreases with the increase of Cr concentration. Both results are consistent with experimental results. An decrease of elastic constants with increasing temperature was also observed in the present work, which is consistent with experimental results. Investigation on elastic properties of defect-containing alloys have shown that vacancies, voids, interstitials and Cr-rich precipitations have different effects on elastic properties of FeCrAl alloys. Vacancies and voids result in the decrease of elastic properties, while interstitials could result in the increase of bulk modulus but decrease of shear modulus. The formation of Cr-rich precipitates increases the elastic properties, which is independent of the number and volume of precipitates. Therefore, the present results indicate that compared to the concentration effect, the radiation defects show different effects on elastic properties. Furthermore, when the radiation effects are predicted, e.g., radiation hardening, not only the contribution from the interaction between dislocation and radiation defects, but also the radiation defects before the interactions with dislocations, should be considered. All these results provide a new understanding to develop and apply the FeCrAl alloy in AFT design.

**Author Contributions:** Conceptualization, N.G. and X.W.; methodology, H.D.; software, M.Y.; validation, M.Y. and N.G.; formal analysis, H.D. and M.Y.; investigation, H.D. and M.Y.; resources, H.D.; data curation, Y.D.; writing—original draft preparation, H.D.; writing—review and editing, N.G. and W.S.; visualization, H.D.; supervision, N.G.; project administration, N.G.; funding acquisition, N.G. All authors have read and agreed to the published version of the manuscript.

**Funding:** This work was funded by the National Natural Science Foundation of China (Grant number. 12075141 and 11675230). WS acknowledges the support provided by the U.S. Department of Energy through the Office of Fusion Energy Sciences (DE-AC05-76RLO-1830).

**Institutional Review Board Statement:** Not applicable.

**Informed Consent Statement:** Not applicable.

**Data Availability Statement:** The data presented in this study are available on request from the corresponding author.

**Conflicts of Interest:** The authors declare no conflict of interest.

#### References

1. Badini, C.; Laurella, F. Oxidation of FeCrAl alloy: Influence of temperature and atmosphere on scale growth rate and mechanism. *Surf. Coat. Technol.* **2001**, *135*, 291–298. [[CrossRef](#)]
2. Han, X.; Wang, Y.; Peng, S.; Zhang, H. Oxidation behavior of FeCrAl coated Zry-4 under high temperature steam environment. *Corros. Sci.* **2019**, *149*, 45–53. [[CrossRef](#)]
3. Briggs, S.A.; Edmondson, P.D.; Littrell, K.C.; Yamamoto, Y.; Howard, R.H.; Daily, C.R.; Terrani, K.A.; Sridharan, K.; Field, K.G. A combined APT and SANS investigation of  $\alpha'$  phase precipitation in neutron-irradiated model FeCrAl alloys. *Acta Mater.* **2017**, *129*, 217–228. [[CrossRef](#)]
4. Park, D.J.; Kim, H.G.; Park, J.Y.; Jung, Y.I.; Park, J.H.; Koo, Y.H. A study of the oxidation of FeCrAl alloy in pressurized water and high-temperature steam environment. *Corros. Sci.* **2015**, *94*, 459–465. [[CrossRef](#)]
5. Wu, X.; Kozłowski, T.; Hales, J.D. Neutronics and fuel performance evaluation of accident tolerant FeCrAl cladding under normal operation conditions. *Ann. Nucl. Energy* **2015**, *85*, 763–775. [[CrossRef](#)]
6. Ukai, S.; Kato, S.; Furukawa, T.; Ohtsuka, S. High-temperature creep deformation in FeCrAl-oxide dispersion strengthened alloy cladding. *Mater. Sci. Eng. A* **2020**, *794*, 139863. [[CrossRef](#)]
7. Terrani, K.A.; Zinkle, S.J.; Snead, L.L. Advanced oxidation-resistant iron-based alloys for LWR fuel cladding. *J. Nucl. Mater.* **2014**, *448*, 420–435. [[CrossRef](#)]

8. Altıparmak, S.C.; Yardley, V.A.; Shi, Z.; Lin, J. Challenges in additive manufacturing of high-strength aluminium alloys and current developments in hybrid additive manufacturing. *Int. J. Lightweight Mater. Manuf.* **2021**, *4*, 246–261. [[CrossRef](#)]
9. Kobayashi, S.; Takasugi, T. Mapping of 475 °C embrittlement in ferritic Fe–Cr–Al alloys. *Scr. Mater.* **2010**, *63*, 1104–1107. [[CrossRef](#)]
10. Edmondson, P.D.; Briggs, S.A.; Yamamoto, Y.; Howard, R.H.; Sridharan, K.; Terrani, K.A.; Field, K.G. Irradiation-enhanced  $\alpha'$  precipitation in model FeCrAl alloys. *Scr. Mater.* **2016**, *116*, 112–116. [[CrossRef](#)]
11. Chang, K.; Meng, F.; Ge, F.; Zhao, G.; Du, S.; Huang, F. Theory-guided bottom-up design of the FeCrAl alloys as accident tolerant fuel cladding materials. *J. Nucl. Mater.* **2019**, *516*, 63–72. [[CrossRef](#)]
12. Gussev, M.N.; Field, K.G.; Yamamoto, Y. Design, properties, and weldability of advanced oxidation-resistant FeCrAl alloys. *Mater. Des.* **2017**, *129*, 227–238. [[CrossRef](#)]
13. Thompson, Z.T.; Terrani, K.A.; Yamamoto, Y. *Elastic Modulus Measurement of ORNL ATF FeCrAl Alloys*; ORNL/TM-2015/632; Materials Science: Oak Ridge, TN, USA, 2015; pp. 1–17.
14. Liu, Z.; Li, Y.; Shi, D.; Guo, Y.; Li, M.; Zhou, X.; Huang, Q.; Du, S. The development of cladding materials for the accident tolerant fuel system from the Materials Genome Initiative. *Scr. Mater.* **2017**, *141*, 99–106. [[CrossRef](#)]
15. Busby, J.T.; Hash, M.C.; Was, G.S. The relationship between hardness and yield stress in irradiated austenitic and ferritic steels. *J. Nucl. Mater.* **2005**, *336*, 267–278. [[CrossRef](#)]
16. Speich, G.; Schwobele, A.; Leslie, W.C. Elastic constants of binary iron-base alloys. *Metall. Trans.* **1972**, *3*, 2031–2037. [[CrossRef](#)]
17. Hellier, A.; Palmer, S.; Whitehead, D. An integrated circuit pulse echo overlap facility for measurement of velocity of sound (applied to study of magnetic phase change). *J. Phys. E Sci. Instrum.* **1975**, *8*, 352. [[CrossRef](#)]
18. Harmouche, M.; Wolfenden, A. Modulus measurements in ordered Co–Al, Fe–Al, and Ni–Al alloys. *J. Test. Eval.* **1985**, *13*, 424–428.
19. Field, K.G.; Briggs, S.A.; Hu, X.; Yamamoto, Y.; Howard, R.H.; Sridharan, K. Heterogeneous dislocation loop formation near grain boundaries in a neutron-irradiated commercial FeCrAl alloy. *J. Nucl. Mater.* **2017**, *483*, 54–61. [[CrossRef](#)]
20. Field, K.G.; Briggs, S.A.; Sridharan, K.; Howard, R.H.; Yamamoto, Y. Mechanical Properties of Neutron-Irradiated Model and Commercial FeCrAl Alloys. *J. Nucl. Mater.* **2017**, *489*, 118–128. [[CrossRef](#)]
21. Garner, F.; Toloczko, M.; Sencer, B. Comparison of swelling and irradiation creep behavior of fcc-austenitic and bcc-ferritic/martensitic alloys at high neutron exposure. *J. Nucl. Mater.* **2000**, *276*, 123–142. [[CrossRef](#)]
22. Liao, X.; Gong, H.; Chen, Y.; Liu, G.; Liu, T.; Shu, R.; Liu, Z.; Hu, W.; Gao, F.; Jiang, C.; et al. Interatomic potentials and defect properties of Fe–Cr–Al alloys. *J. Nucl. Mater.* **2020**, *541*, 152421. [[CrossRef](#)]
23. Miller, A.; Saunders, G.; Yagurtcu, Y. Pressure dependences of the elastic constants of PbTe, SnTe and Ge<sub>0.08</sub>Sn<sub>0.92</sub>Te. *J. Phys. C Solid State Phys.* **1981**, *14*, 1569. [[CrossRef](#)]
24. Xu, S.; Xie, D.; Liu, G.; Ming, K.; Wang, J. Quantifying the resistance to dislocation glide in single phase FeCrAl alloy. *Int. J. Plast.* **2020**, *132*, 102770. [[CrossRef](#)]
25. Voight, W. *Lehrbuch der Kristallphysik*; Teubner: Leipzig, Germany, 1928.
26. Yeom, H.; Maier, B.; Johnson, G.; Dabney, T.; Walters, J.; Sridharan, K. Development of cold spray process for oxidation-resistant FeCrAl and Mo diffusion barrier coatings on optimized ZIRLO™. *J. Nucl. Mater.* **2018**, *507*, 306–315. [[CrossRef](#)]
27. Yamamoto, Y.; Sun, Z.; Pint, B.A.; Terrani, K.A. *Optimized Gen-II FeCrAl Cladding Production in Large Quantity for Campaign Testing*; Oak Ridge National Laboratory: Oak Ridge, TN, USA, 2016.
28. Wang, R.; Zhang, X.; Wang, H.; Ni, J. Phase diagrams and elastic properties of the Fe–Cr–Al alloys: A first-principles based study. *Calphad* **2019**, *64*, 55–65. [[CrossRef](#)]
29. Leibfried, G.; Ludwig, W. *Theory of Anharmonic Effects in Crystals, Solid State Physics*; Elsevier: Amsterdam, The Netherlands, 1961; pp. 275–444.
30. Li, D.Z.; Zhang, X.D.; Li, J.; Zhao, L.J.; Wang, F.; Chen, X.Q. Insight into the elastic anisotropy and thermodynamics properties of Tantalum borides. *Vacuum* **2019**, *169*, 108883. [[CrossRef](#)]